Chemical Engineering Science 121 (2015) 77–86

Contents lists available at ScienceDirect

Chemical Engineering Science

journal homepage: www.elsevier.com/locate/ces

Crystal structure, stability, and electronic properties of hydrated metal sulfates $MSO_4(H_2O)_n$ (M=Ni, Mg; n=6, 7) and their mixed phases: A first principles study

Changming Fang [a], Xiaoqian Lu [b], Wim Buijs [b], Zhaochuan Fan [b], Fatma Elif Genceli Güner [b], Marijn A. van Huis [a], Geert-Jan Witkamp [c], Thijs J.H. Vlugt [b,*]

[a] Soft Condensed Matter, Debye Institute for Nanomaterials Science, Utrecht University, Princetonplein 5, 3584 CC Utrecht, The Netherlands
[b] Process & Energy Department, Delft University of Technology, Leeghwaterstraat 39, 2628 CB Delft, The Netherlands
[c] Department of Biotechnology, Delft University of Technology, Julianalaan 67, 2628 BC Delft, The Netherlands

HIGHLIGHTS

- Periodic OptB86-vdW-GGA+U DFT calculations for hydrated M(II) sulfates.
- A comparative study by cluster B3LYP/6-31G* DFT calculations.
- Formation of continuous solid solution for 6- and 7-hydrated Ni/Mg sulfates.
- Calculation of electronic band gaps for 6- and 7-hydrated Ni/Mg sulfates.

ARTICLE INFO

Article history:
Received 29 April 2014
Received in revised form
27 June 2014
Accepted 12 July 2014
Available online 17 July 2014

Keywords:
Hydrated metal (II) sulfates
Density functional theory
Crystal structure
Phase stability
Electronic structure

ABSTRACT

Removal of Mg from hydrated Ni sulfates has long been a problem in the industrial purification process of hydrated Ni sulfates. In this work, we have investigated this industrial problem using state-of-the-art molecular simulations. Periodic Density Functional Theory (DFT) and cluster DFT calculations are used to study the crystal structures and phase stability of the hexahydrated and heptahydrated Ni and Mg sulfates and their mixed phases. The calculated lattice parameters of $MSO_4(H_2O)_n$ (M=Ni, Mg; n=6, 7) crystals are in good agreement with available experimental data. The relative energy differences of the mixed phase for both hexahydrated and heptahydrated Ni/Mg sulfates obtained from both the periodic and cluster DFT calculations are generally less than kT (25.8 meV, T=300 K), indicating that a continuous solid solution is formed. We also investigated the Bader charges and electronic structures of the hexahydrated and heptahydrated Ni/Mg sulfates using the periodic DFT calculations. The energy band gaps of the hexahydrated and heptahydrated Ni and Mg sulfates were predicted by first-principles calculations. Large energy band gaps of about ~5.5 eV were obtained from the DFT–GGA calculations for hydrated Mg sulfates, and band gaps of about ~5.1 eV were obtained by the DFT–GGA+U calculations for hydrated Ni sulfates.

1. Introduction

Hydrated metal (II) sulfates, $MSO_4(H_2O)_n$ (M=Ni, Mg; n=1–11) are widely used in different industrial processes. For instance, $NiSO_4(H_2O)_n$-based solutions are commonly used in nickel plating, surface coating, super-capacitors, and highly efficient photocatalysts production (Patterson, 1994; Lascelles et al., 2005; Carja et al., 2011; Dar et al., 2013). While also being produced from nickel and copper ore as a side product, most part of nickel sulfate is recovered from recycling products containing nickel. For producing solid phase nickel sulfate for commercial sale, crystallization is obligatory as the last step during producing process (Ramachandran et al., 1991; Abbas et al., 2002; Moldoveanu and Demopoulos, 2002) and highly pure nickel sulfate is usually required in applications. Among the most common impurities in solid nickel sulfate heptahydrate products, Mg is one impurity which is difficult to be removed because of the isomorphous replacement between Mg and Ni in $MSO_4(H_2O)_7$ (Smolik, 2000). Recent work on eutectic freeze crystallization showed that nickel sulfate heptahydrate can be recovered from industrial nickel sulfate streams with high purity, except for an accumulated Mg uptake in $NiSO_4(H_2O)_7$ crystals (Lu et al., 2014a,b). Afterwards, recrystallization of $NiSO_4(H_2O)_7$ obtained from eutectic

* Corresponding author.
E-mail address: t.j.h.vlugt@tudelft.nl (T.J.H. Vlugt).

http://dx.doi.org/10.1016/j.ces.2014.07.026
0009-2509/

freezing crystallization into $NiSO_4(H_2O)_6$ was used as a further purification process to remove Mg impurity. But according to experimental results (Lu et al., 2014a,b), this recrystallization process is a solvent mediated process, which means that the impurity content of Mg in the recrystallization liquid highly affects the final quality of product $NiSO_4(H_2O)_6$.

Hydrated metal (II) sulfates are not only of industrial interest, but are also commonly studied as model systems for their fundamental physical and chemical properties (Cox et al., 1955; Baur, 1964; Zalkin et al., 1964; Wells, 1984; Maneva et al., 1990; Koga and Tanaka, 1994; Patterson, 1994; Nesbitt et al., 2000; Squyres et al., 2004; Lascelles et al., 2005; Delorme et al., 2009; Grevel and Majzlan, 2009; Nordstrom, 2009; Hawthorne, 2012; Dar et al., 2013). The crystal structures and chemical bonds of Mg and Ni sulfate hexahydrates were measured by X-ray diffraction (Zalkin et al., 1964; Ptasiewicz-Bak et al., 1993) and an ionic model of $[Ni(H_2O)_6]^{2+}(SO_4)^{2-}$ was proposed for $NiSO_4(H_2O)_6$ (Ptasiewicz-Bak et al., 1993). Schlapp and Penney (1932) pointed out that, for a Ni^{2+} ion surrounded by an octahedron of negative ions or water molecules, the ground orbital state is a singlet. However, later this turned out to be erratic: all hydrated nickel sulfates and nitrates are paramagnetic (Swift and Connick, 1962). The magnetic properties of $NiSO_4(H_2O)_6$ have been intensively investigated by different experimental techniques (Schlapp and Penney, 1932; O'Connor et al., 1941; Watanabe, 1962; Stout and Hadley, 1964; Fisher et al., 1967; Pontusch et al., 1973). O'Connor et al. (1941) explored the magnetic rotatory power of $NiSO_4(H_2O)_6$ in the ultraviolet region. The magnetic susceptibility of single crystalline $NiSO_4(H_2O)_6$ and $NiSO_4(H_2O)_7$ were measured in the temperature range between liquid He and room temperature (Watanabe, 1962). From the specific heat measurements of $NiSO_4(H_2O)_6$ single crystals between 1 K and 20 K, a peak was observed at 2.58 K (Stout and Hadley, 1964). Particularly important for our study is the work of Benrath and Neumann (1939), who provided experimental evidence for the formation of a solid solution of $Ni_xMg_{1-x}SO_4(H_2O)_n$ (x=0–1; n=6, 7). In addition, $Ni_{0.4}Mg_{0.6}SO_4(H_2O)_6$ was reported being found in nature (Osborne, 1947).

The number of theoretical studies on Mg sulfate hydrates is limited. The thermoelastic properties of $MgSO_4(H_2O)_7$ were recently studied using the density functional theory with generalized gradient approximation (DFT–GGA) (Fortes et al., 2006). Luo et al. (2013) investigated absorption of water on $MgSO_4$ surfaces using GGA–DFT with the ultrasoft pseudopotential method. Separations between Mg and O surface atoms after water adsorption were observed in their modeling which indicated that deliquescence occurs on the $MgSO_4$ surfaces (Luo et al., 2013). Maslyuk et al. (2005) calculated the crystal structure of $MgSO_4 \cdot H_2O$ using a combination of DFT and semiempirical methods, while the electronic structure of $MgSO_4H_2O$ was calculated by a hybrid density functional theory-Hartree–Fock (DFT-HF) approach. The calculated band gap for $MgSO_4H_2O$ was 7.77 eV, which is in agreement with the experimentally determined band gap of 7.4 eV (Maslyuk et al., 2005). The configurations of isolated $MgSO_4(H_2O)_n$ (n=1, 5) molecules were optimized at a DFT PW91-TZ2P level (Iype et al., 2012). A proton transfer was found in $MgSO_4(H_2O)_6$ (Iype et al., 2012), which we believe is an unrealistic erroneous result due to the single $MgSO_4(H_2O)_6$ molecule chosen in these calculations (see our discussion in Section 2.2).

First-principles studies on Ni sulfate hydrates are even rarer in literature (Schröder et al., 2011). This is probably because of the difficulties in dealing with the Ni 3d state in the Ni-contained compounds. The relatively large systems of $MSO_4(H_2O)_n$ ($\sim$100 atoms/unit cell) also make the computations very time-consuming. Due to the presence of the water molecules in the system, describing the dispersion interactions by DFT calculations is also difficult.

In this work, we study the crystal structure, phase stability and electronic structures of Ni and Mg sulfate hexahydrates and heptahydrates using state-of-the-art molecular simulations. The purpose of this study is threefold:

1. We are looking for a definite answer to the question which is arousing the interest of the hydrometallurgy industry: Can Mg incorporation in $NiSO_4$ products be prevented by recrystallization? Or do hydrated Ni and Mg sulfates form a continuous solid solution as suggested by Benrath and Neumann (1939)?
2. As mentioned above, first principles calculations on the hydrated Ni/Mg sulfates are very challenging. Using a combination of state-of-the-art energy functionals in the periodic DFT calculations, we aim to provide a trustful description of the physical interactions.
3. We are also exploring another molecular modeling approach, the DFT cluster calculations, which require less computational power and are therefore able to simulate larger systems or to shorten the simulation time. A comparison between the periodic and cluster DFT calculations will be made.

The paper is structured as follow. Section 2 introduces the methods used in the periodic and cluster DFT calculations in detail. The crystals structures and the cluster models are also introduced. Section 3.1 presents the crystal structures and chemical bonding of hexahydrated and heptahydrated Ni/Mg sulfates calculated by both the periodic and cluster DFT calculations. Section 3.2 shows a comparison of the periodic and cluster DFT calculations of the relative stability of the $Ni_xMg_{1-x}SO_4(H_2O)_n$ (n=6, 7). Sections 3.3 and 3.4 discuss Bader charges of atoms and the electronic structure of the $MSO_4(H_2O)_n$ from the periodic DFT calculations, respectively. Our conclusions are summarized in Section 4.

2. Methods

2.1. Periodic density functional theory calculations

In periodic DFT calculations, the projector-augmented wave (PAW) method (Blochl, 1994; Kresse and Joubert, 1999) was adopted. The first-principles code Vienna Ab-initio Simulations Package (VASP) (Kresse and Hafner, 1993, 1994) was employed for the structural optimizations and the electronic structure calculations. A nonlocal van der Waals density functional, optB86-vdW, was used in combination with the generalized gradient approximation (GGA) (Dion et al., 2004; Klimes et al., 2010, 2011) to describe the exchange and correlation energy terms. This choice is based on two considerations: First, this newly developed correlation functional is based on the GGA approximation (Perdew et al., 1996) with the integration of the dispersion interactions, which is able to describe the hydrogen bonds of the water in the hydrated metal sulfates. Second, it has been established that GGA offers a better description of (spin-polarized) transition metals and compounds compared to the local (spin-polarized) density approximation (LDA), and it provides energetics of the compounds quite well (Amador et al., 1992; Fang et al., 2010). However, it is well known that the standard density functionals such as LDA and GGA fail to describe localized states (e.g. the Ni 3d states in NiO and $NiSO_4$) (Hubbard, 1963; Sawatzky and Allen, 1984; Madsen and Novak, 2005; Larsson, 2006). This deficiency can be solved by describing the on-site interactions of the localized 3d states with a simple parameter, the Hubbard U (Hubbard, 1963) with U=5.96 eV for Ni 3d in NiO (Madsen and Novak, 2005).

The crystal models of $MSO_4(H_2O)_n$ (M=Ni, Mg; n=6,7) were constructed on the basis of the available experimental data (Frondel and Palache, 1949; Baur, 1964; Zalkin et al., 1964;

Kavitha and Mahadevan, 2013). For the $MSO_4(H_2O)_6$, two different phases, i.e. T (space group: $P4_12_12$) and m (space group: $C2/c$), were taken into consideration. Although the T-$MgSO_4(H_2O)_6$ and m-$NiSO_4(H_2O)_6$ are not stable in nature, their lattice parameters can be obtained by DFT optimization of Ni- and Mg-substituted T-$NiSO_4(H_2O)_6$ and m-$MgSO_4(H_2O)_6$ unit cells, respectively. Beside the hydrated metal sulfates, several related compounds were also studied through the periodic DFT calculations for validation and comparison. These related compounds include MO, α- and β-MSO_4, and ice_XI. The crystal structures of all materials involved are shown in Fig. 1.

In the periodic DFT calculations, we used a cut-off energy of 600 eV for the wave functions and 850 eV for the augmentation functions. These high cut-off energies are necessary to accurately describe the localized Ni 3d states and the O 2p–S 3p and O sp–H 1s strong-bonding in the compounds. The electronic wave functions were sampled on a $6\times6\times2$ Monkhorst–Pack (MP) grid (Monkhorst and Pack, 1976) with 18–36 k-points and a $8\times4\times4$ MP grid with 16–64 k-points in the irreducible Brillouin zone (BZ) for the T-$MSO_4(H_2O)_6$ and O-$MSO_4(H_2O)_7$ phases, respectively. For the calculations of local electronic configurations and partial density of states of the atoms, the Wigner–Seitz (WS) radius was set as 1.2 Å for Ni and Mg, 0.9 Å for O and S and 0.4 Å for H, respectively. Note that the 3d electrons of the Ni atom exhibit an itinerant character in the metals and their compounds, in principle belonging to the whole crystal. However, we can decompose the plane waves in the atomic WS sphere and obtain Ni 3d components in the spheres for both the spin-up (or majority) and spin-down (minority) directions. In this way, a local magnetic moment is obtained from the difference between the number of spin-up and spin-down electrons in the WS sphere. The choices of the MP k-meshes and cut-off energies are based on convergence tests in which the energy convergence is kept below 1 meV/atom.

2.2. Cluster density functional theory calculations

The commercially available Spartan 14 package (Wavefunction Inc., Irvine, California, USA. www.wavefun.com) was used for all cluster calculations. The routine B3LYP/6-31G* for DFT calculations

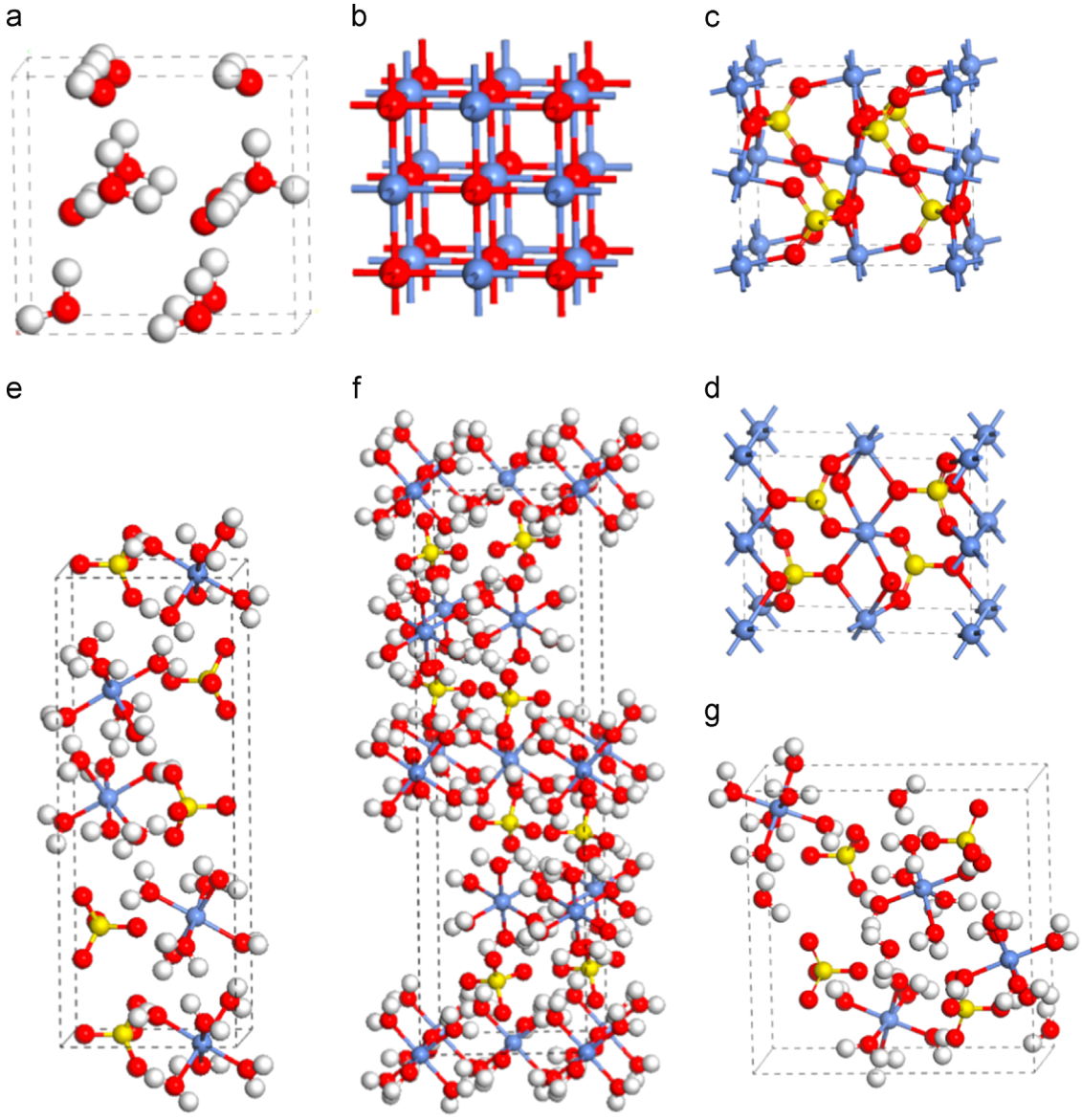

Fig. 1. Schematic representation of crystal structures for (a) ice_XI, (b) MO, (c) α-MSO_4, (d) β-MSO_4, (e) T-$MSO_4(H_2O)_6$, (f) m-$MSO_4(H_2O)_6$, (g) $MSO_4(H_2O)_7$. The white, red, gray, and yellow spheres are H, O, M (Ni or Mg), and S, respectively. (For interpretation of the references to color in this figure legend, the reader is referred to the web version of this article.)

were used. Despite its known incapability of describing particularly van der Waals interactions correctly, or depicting electronic (fine) structure more generally, both energies and geometrical structures are usually reproduced quite well (Hehre, 2003). Typical bond length errors are less than 0.02 Å. All metal sulfate hydrates display strong static electrostatic behavior, both in the $M(H_2O)_6$ cation and the sulfate anion, which should be adequately covered by B3LYP. Furthermore, by direct comparison of the total energies of very similar complexes, a cancellation of possible errors in the van der Waals interactions can be expected. Finally, it should be noted that the cluster calculations presented herein are only to be used for comparing their relative energies and geometries, but not for the determination of bulk electronic structure features of the solid state materials.

To set up meaningful comparisons with respect to geometry and total energy, clusters were selected from the known crystal structures of both $MgSO_4(H_2O)_6$ and $NiSO_4(H_2O)_7$. Fig. 2b shows a tetrameric cluster from the unit cell of T-$MgSO_4(H_2O)_6$ containing four $Mg(H_2O)_6^{2+}$ cations and four sulfates. Geometry optimization of this tetrameric cluster leads to proton transfer from the M coordinated water molecules to the sulfate anion. The same type of proton transfer was reported also by Iype et al. (2012) using a different DFT code. However, obviously this is an erroneous result due to the fact that the cluster shows a too large charge separation between the $Mg(H_2O)_6^{2+}$ cations and the sulfate anions at the border of the parent unit cell. The crystal structure does not show an indication for such a proton transfer. Therefore, we took the dimeric cluster for $MgSO_4(H_2O)_6$ (see Fig. 2c), wherein the two sulfates are stabilized by H-bridges of the water molecules coordinated to the M^{2+} cations. In case of $NiSO_4(H_2O)_7$, the tetrameric unit cell could be directly chosen (see Fig. 2d), as inside this unit cell there is sufficient hydrogen bridging towards the sulfate anions to avoid the previously-mentioned proton transfer.

3. Results and discussion

3.1. Structures and chemical bonds

Before discussing the hydrated Ni and Mg sulfates, we discuss the periodic DFT calculations on several reference compounds (MO, α- and β-MSO_4, and ice_XI) for validation and comparison. Table 1 lists the lattice parameters of these compounds calculated using the periodic DFT calculations in comparison with available experimental data. In general, the calculated lattice parameters of all the related compounds are in good agreement with experimental data with deviations less than 4%. Therefore, the computational schemes used here are suitable for the studies of these reference compounds, thus, are also expected to be suited to the hydrated Ni and Mg sulfates and their mixed phases.

The lattice parameters of m-$MSO_4(H_2O)_6$, T-$MSO_4(H_2O)_6$, and $MSO_4(H_2O)_7$ obtained from the periodic DFT calculations are listed in Table 2 together with available experimental data. The computed lattice parameters for all the hydrated Ni and Mg sulfates phases show good agreement with the available experimental data. The highest deviation from the experimental data is 3.1% in the length of the *a*-axis of O–$MgSO_4(H_2O)_7$ (Epsom salt). Table 3 shows the chemical bond lengths in these hydrated Ni and Mg sulfates and their related compounds from the periodic DFT calculations. In all the solid phases, both Ni and Mg atoms/ions are in an octahedral coordination with oxygen atoms/ions, with bond-lengths of about 1.99–2.25 Å for Mg–O and 1.99–2.21 Å for Ni–O. In both Mg and Ni sulfates, each S atom/ion is tetragonally coordinated by four oxygen atoms/ions with the S–O interatomic distances ranging from 1.46 to 1.52 Å, revealing a high stability of $(SO_4)^{2-}$ clusters in the ionic model. The calculated O–H bond lengths vary slightly around 0.99 Å.

In line with the periodic DFT calculations, structural optimizations of the hydrated metal sulfate clusters by cluster DFT calculations yield octahedral $Ni(H_2O)_6^{2+}$ and $Mg(H_2O)_6^{2+}$ cations, as well as sulfate anions. Fig. 2a shows both the octahedral coordination in $Ni(H_2O)_6^{2+}$ and $Mg(H_2O)_6^{2+}$ and the triplet spin state of the simple $Ni(H_2O)_6^{2+}$ cation. The volumes of these two cations are 118.08 Å^3, and 119.54 Å^3 respectively, which differ less than 1%. Consequently, Mg–O bonds are slightly larger than Ni–O bonds: Mg–O = 2.120 Å and Ni–O = 2.077 Å. This similarity in shape and volume can be considered as an indication for a continuous solid solution.

The average Ni–O bond length of the dimeric clusters $(MSO_4(H_2O)_6)$ is slightly larger than the Ni–O bond length in the crystal structure: 2.083 Å (cluster) vs 2.051 Å (crystal). For the S–O bond lengths a similar observation can be obtained: 1.520 Å (cluster) vs 1.481 Å (crystal). Mg–O distances in the clusters are 2.111 Å. In the full Ni cluster the Ni–Ni atomic distance is 6.258 Å, while in the full Mg cluster the Mg–Mg atomic distance is 6.286 Å. The volumes of the dimeric clusters are in line with the bond length observations: the volume of the dimeric Ni cluster is 375.52 Å^3 while the volume of dimeric Mg cluster is 379.12 Å^3. Ni and Mg dimeric clusters have a similar geometry.

As is shown in Fig. 2d, the B3LPY-optimized $NiSO_4(H_2O)_7$ tetrameric structure shows a slightly decreased volume compared to the initial unit cell, due to the lack of attractions from the surrounding atoms which are no longer present in the cluster. It can be concluded that the cluster calculation yields correct results with respect to the overall spin state of the tetrameric $Ni(H_2O)_7SO_4$ with 8 unpaired electrons (Swift and Connick, 1962). The results are in line with the literature which states that all $Ni(H_2O)_nSO_4$ phases are paramagnetic (Swift and Connick, 1962). As is shown in Table 3, the average Ni–O bond length of the B3LYP-optimized cluster is slightly larger than the Ni–O bond length in the crystal structure: 2.078 Å (cluster) vs 2.065 Å (crystal). For the S–O bond lengths a similar observation can be made: 1.520 Å (cluster) vs 1.488 Å (crystal). The average Ni–Ni distance is 6.504 Å in the crystal and 5.546 Å for the optimized cluster. The volumes of the clusters are: $V_{crystal} = 862.97$ Å^3 and $V_{optimized\text{-}cluster} = 826.48$ Å^3, the latter being considerably smaller than the former. The main reason for the much lower volume of the optimized cluster is, the rather large displacement of the four free water molecules from the side of the crystal towards the inside of the cluster. This can be explained by the fact that contrary to the real crystal, the cluster does not see its neighboring cells.

The B3LYP-optimized full Mg clusters yield similar results as the full Ni clusters (Table 3). The average Mg–O bond length of the full Mg tetrameric cluster is 2.110 Å while the average from the periodic DFT calculations is 2.080 Å. The average S–O bond lengths are again 1.520 and 1.488 Å from the cluster and periodic DFT calculations, respectively. The average Mg–Mg distance is 5.631 Å. The volume of the full Mg cluster is 834.38 Å^3, slightly larger than the volume of the all Ni-cluster.

3.2. Phase stabilities

In order to assess the relative stability of the mixed phases $(Ni_xMg_{1-x})SO_4(H_2O)_n$ ($x = 0-1$; $n = 6, 7$), the relative energy difference (ΔE) is defined as

$$\Delta E\left[(Ni_xMg_{1-x})SO_4(H_2O)_n\right] = E\left[(Ni_xMg_{1-x})SO_4(H_2O)_n\right] - x\,E\left[NiSO_4(H_2O)_n\right] - (1-x)\,E\left[MgSO_4(H_2O)_n\right])$$

Here, the relative energy difference ΔE and the absolute energy E could either be the formation energy in the periodic DFT calculations or the total energy in the cluster DFT calculations.

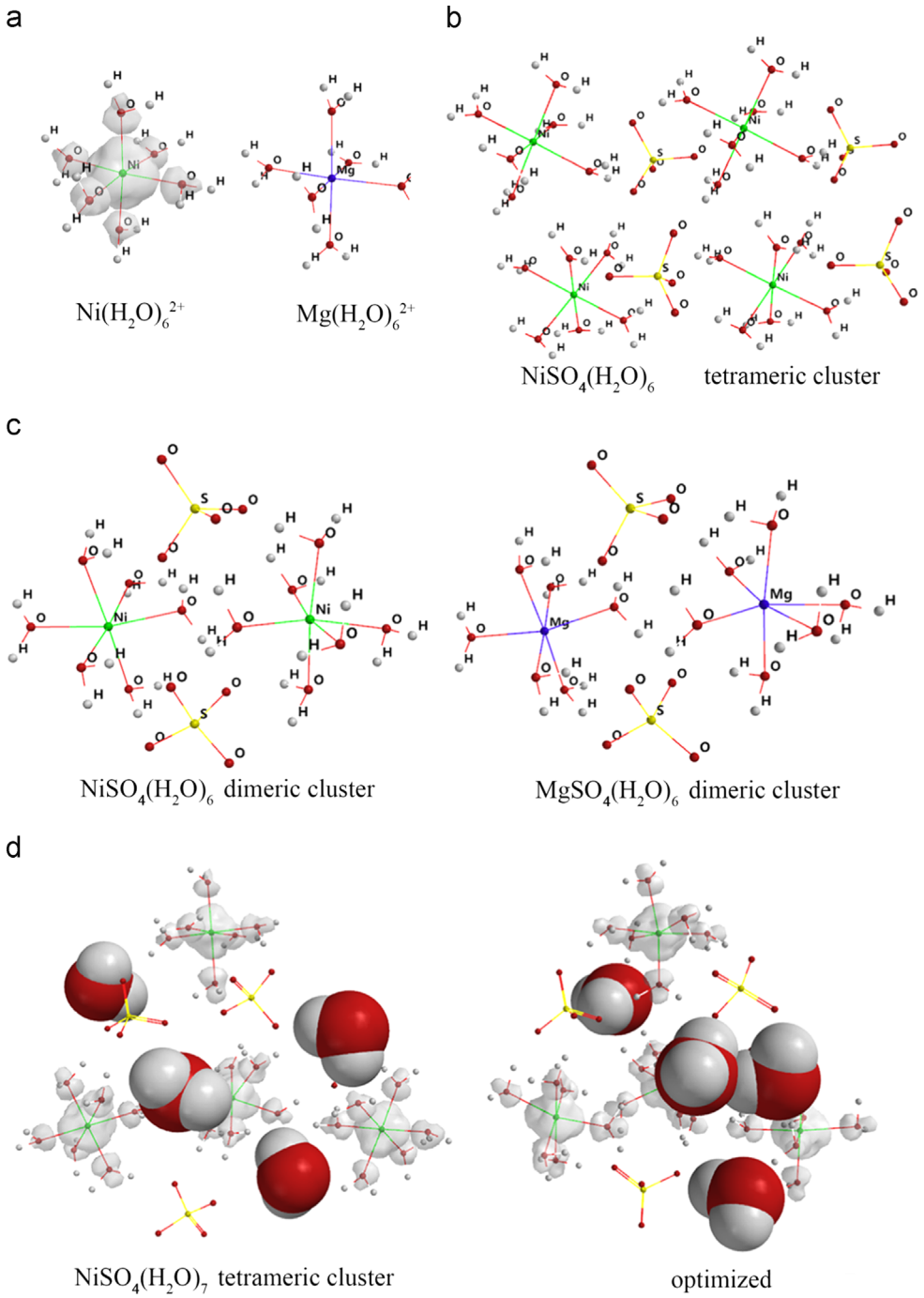

Fig. 2. Constructed and B3LYP-optimized clusters of (a) $Ni(H_2O)_6^{2+}$ and $Mg(H_2O)_6^{2+}$ with spin densities on $Ni(H_2O)_6^{2+}$ (0.002e/au^3), (b) optimized tetrameric $NiSO_4$, (c) dimeric $MSO_4(H_2O)_6$ clusters, (d) unit cell of $NiSO_4(H_2O)_7$ (left) and optimized tetrameric cluster (right) with spin densities on $Ni(H_2O)_6^{2+}$ (0.002 e/au^3). The white, red, green, purple, and yellow spheres are H, O, Ni, Mg, and S, respectively. Four free water molecules (see the main text) are shown in the vdW presentation. (For interpretation of the references to color in this figure legend, the reader is referred to the web version of this article.)

In the periodic DFT calculations, considering the strong similarity of local structures between the T and m phases, only the T-$MSO_4(H_2O)_6$ structure was considered for the stability comparison of the hexahydrate Ni and Mg sulfates. In the hydrate metal sulfates, the distances between metal atoms/ions are very large, typically larger than 5 Å. Such long metal–metal distances indicate weak exchange interactions and small energy differences between different configurations. Therefore, only one possible configuration of the $(Ni_xMg_{1-x})SO_4(H_2O)_n$ mixed phase was calculated. At 0 K, the enthalpy difference is equal to the energy difference, $\Delta G = \Delta E$, where we ignore the zero-point vibration contribution.

The relative Gibbs free energy difference for $(Ni_xMg_{1-x})SO_4(H_2O)_n$ (n=6, 7) obtained by the periodic DFT calculations are shown in Fig. 3. Note that the density-functional theory only works for the ground states of materials, i.e. it describes the total valence electron energy at 0 K. As shown in Fig. 3, the relative energy differences of the mixed phases with respect to the pure hydrate metal sulfates at 0 K are rather small (typically about a few meV/f.u.). This can be understood as the consequence of the long atomic distances and the weak exchange interactions between metals. These results are in line with experiments that a magnetic ordering occurs at very low temperatures (2–3 K) (Maslyuk et al., 2005).

Table 1
Calculated lattice parameters for ice_XI, MgO, $MgSO_4$, NiO, and $NiSO_4$ from the periodic DFT calculations and available experimental data. The lattice parameters *a*, *b* and *c* are in Å.

Compound	Space group (Nr.)	Bulk calc.	Exp.
Ice_XI	*Cmc2₁* (36)		
	a	4.343	4.5019[a]
	b	7.609	7.7978[a]
	c	7.035	7.3280 [a]
MgO	*Fm-3m* (225)		
	a	4.235	4.13[b]
α-$MgSO_4$	*Cmcm* (63)		
	a	5.223	5.1686 [c]
	b	7.863	7.8678 [c]
	c	6.442	6.5667 [c]
β-$MgSO_4$	*Pnma* (62)		
	a	8.654	8.5817 [c]
	b	6.667	6.6727 [c]
	c	4.743	4.7343 [c]
NiO	*Fm-3m* (225)		
	a	4.156/4.203[g]	4.1705 [d]
α-$NiSO_4$	*Cmcm* (63)		
	a	5.196/5.195 [g]	5.188 [e], 5.155 [f]
	b	7.840/7.816 [g]	7.848 [e], 7.842 [f]
	c	6.267/6.290 [g]	6.300 [e], 6.338 [f]
β-$NiSO_4$	*Pnma* (62)		
	a	8.615/8.613 [g]	
	b	6.460/6.464 [g]	
	c	4.720/4.721 [g]	

[a] Experimental report in Leadbetter et al. (1985).
[b] Experimental report in Wyckoff (1921).
[c] Experimental report in Fortes et al. (2007) (at 4.2 K).
[d] Experimental report in Bartel and Morosin (1971) (extended to 0 K).
[e] Experimental report in Wildner (1990).
[f] Experimental report in Frazer and Brown (1962).
[g] DFT+*U* with *U*=5.96 eV (see main text).

Table 2
Calculated lattice parameters for hydrated metal sulfates from the periodic DFT calculations and available experimental data. The lattice parameters *a*, *b* and *c* are in Å.

Compound	Space Group (Nr.)	Calc.	Exp.
m-$MgSO_4$:$(H_2O)_6$ (Hexahydrite)	*C2/c* (15)		
	a	9.883	10.110[a]
	b	7.282	7.212[a]
	c	24.005	24.41[a]
	β	98.34°	98.30°[a]
T-$MgSO_4(H_2O)_6$	$P4_12_12$ (92)		
	a	6.794	–
	c	18.068	
$MgSO_4$:$(H_2O)_7$ (Epsom salt)	*Cmcm* (63)		
	a	6.646	6.858[b]
	b	11.810	11.86[b]
	c	11.943	11.99[b]
m-$NiSO_4$:$(H_2O)_6$	*C2/c* (15)		
	a	9.830/9.845[e]	–
	b	7.102/7.238 [e]	
	c	23.416/24.025[e]	
	β	98.67°/98.70° [e]	
T-$NiSO_4$:$(H_2O)_6$ (Retgersite)	$P4_12_12$ (92)		
	a	6.755/6.761 [e]	6.765[c]
	c	17.936/18.002 [e]	18.20[c]
$NiSO_4$:$(H_2O)_7$ (Morenosite)	*Cmcm* (63)		
	a	6.601/6.608 [e]	6.712[d]
	b	11.737/11.758 [e]	11.8[d]
	c	11.863/11.861 [e]	11.99[d]

[a] Experimental report in Zalkin et al. (1964).
[b] Experimental report in Baur (1964).
[c] Experimental report in Frondel and Palache (1949).
[d] Experimental report in Kavitha and Mahadevan (2013).
[e] DFT+*U* with *U*=5.96 eV (see main text).

At elevated temperatures, configuration entropy plays a more important role in the free energy of the system. The weak interactions between the metal ions suggest that a random model for the configurations for the alloying phases can be used as a correction for the Gibbs free energy calculations. We considered a unit cell containing four metal ions. The configuration number (*W*) for one unit cell is 4 for $Ni_{0.25}Mg_{0.75}SO_4(H_2O)_n$ and $Ni_{0.75}Mg_{0.25}SO_4(H_2O)_n$, and is 6 for $Ni_{0.5}Mg_{0.5}SO_4(H_2O)_n$. The correction of the configuration entropy, $S=k\ln W$ (per unit cell), was included to estimate the free energies of the mixed phases at finite temperatures. It is suggested in Fig. 3 that the mixed phases with different fractions of Ni can be formed at room temperature (300 K). Note that our calculations also show an unstable $(Ni_{0.25}Mg_{0.75})SO_4(H_2O)_7$ phase with a relatively large positive energy difference (~11 meV/f.u.). Considering the small energy differences (~40 meV) and the large number (88–108) of atoms per unit cell, we believe this exception is just a marginally numerical error. The result of our periodic DFT calculations indicates that it is difficult to obtain hydrated Ni sulfate of high purities by recrystallizing Ni sulfates liquids with Mg^{2+} contamination at ambient conditions.

The typical computing time for a similar system (same number of atoms) by the cluster DFT calculations (about one day for a tetrameric cluster) is one tenth of that by the periodic DFT calculations (more than one week for one unit cell). Therefore, we investigated the relative stabilities of a mixed phase of hydrate metal sulfates with more possible configurations in the cluster DFT calculations. For the mixed phases of the dimeric clusters (hexahydrate metal sulfates), both possible $Ni_{0.5}Mg_{0.5}(H_2O)_6SO_4$ configurations were chosen, while for the mixed phases of the tetrameric clusters (heptahydrate metal sulfates), all possible four $Ni_{0.75}Mg_{0.25}(H_2O)_7SO_4$ clusters, one $Ni_{0.5}Mg_{0.5}(H_2O)_7SO_4$ clusters, and one $Ni_{0.25}Mg_{0.75}(H_2O)_7SO_4$ clusters were chosen for full optimization and energy calculation. In the $Ni_{0.5}Mg_{0.5}(H_2O)_6SO_4$ dimeric clusters, the averaged Ni–Mg distance in the mixed clusters is 6.260 Å, slightly larger than the Ni–Ni distance (6.258 Å) in the full Ni dimeric cluster and smaller than the Mg–Mg distance (6.286 Å) in the full Mg dimeric cluster. The optimized volume of these $Ni_{0.5}Mg_{0.5}(H_2O)_6SO_4$ clusters (377.20 $Å^3$) is also between that of the full Ni dimeric cluster (375.52 $Å^3$) and the full Mg dimeric cluster (379.12 $Å^3$). All of them are very similar, but increase with Mg concentration. In the optimized mixed phases of the tetrameric clusters, the average Ni–O bond length in the various clusters is 2.078 Å, The average Mg–O bond length is 2.110 Å, and the average S–O bond length is 1.520 Å. The calculated volumes of the $Ni_{0.75}Mg_{0.25}(H_2O)_7SO_4$, $Ni_{0.5}Mg_{0.5}(H_2O)_7SO_4$, and $Ni_{0.25}Mg_{0.75}(H_2O)_7SO_4$ clusters are 828.26 (averaged), 830.80, and 832.42 $Å^3$, respectively, perfectly in line with the results for the all Ni- and all Mg-clusters. It is important to note that all 6 clusters remain visually intact, however slightly increasing in volume with increasing Mg-content. The larger deviation of the volume of the $M(H_2O)_7(SO_4)$ clusters from the original unit cell is due to the displacement of the seventh water molecule from the outside to the inside of the cluster, still maintaining the relative position of the octahedral $M(H_2O)_2^{2+}$ cation and the sulfate anion.

From cluster DFT calculations, it is clear that size and volume of the simple cations $Mg(H_2O)_2^{2+}$ and $Ni(H_2O)_2^{2+}$ are very similar, the former being slightly larger (~1%). This behavior is consistently shown for the various dimeric and tetrameric clusters. However, cluster calculations cannot answer the question if partial or full isomorphous substitution of $Ni(H_2O)_2^{2+}$ by $Mg(H_2O)_2^{2+}$ is

Table 3
Calculated chemical bonds in hydrated metal sulfates and related compounds from both periodic and cluster DFT calculations. All bond lengths are in Å.

Phase	Bonds	Periodic DFT calc.	Cluster DFT calc.
Ice_XI	H–O	1.01 (× 2)	–
MgO	Mg–O	2.14 (× 6)	–
NiO	Ni–O	2.08 (× 6)	–
α-$MgSO_4$	Mg–O	2.03 (× 2), 2.14 (× 4)	–
	S–O	1.46 (× 2), 1.51 (× 2)	
α-$NiSO_4$	Ni–O	2.02 (× 2), 2.10 (× 4)	–
	S–O	1.46 (× 2), 1.52 (× 2)	
β-$MgSO_4$	Mg–O	1.99 (× 2), 2.11 (× 2), 2.25 (× 2)	–
	S–O	1.46 (× 2), 1.49, 1.50	
β-$NiSO_4$	Ni–O	1.99 (× 2), 2.06 (× 2), 2.21 (× 2)	–
	S–O	1.46 (× 2), 1.51, 1.52	
m-$MgSO_4$:$(H_2O)_6$	Mg–O	2.06 (× 2), 2.08 (× 2), 2.09 (× 2)	–
	S–O	1.48, 1.49 (× 2), 1.50	
m-$NiSO_4$:$(H_2O)_6$	Ni–O	2.06 (× 2), 2.07 (× 2), 2.08 (× 2)	–
	S-O	1.48, 1.49 (× 2), 1.50	
T-$MgSO_4$:$(H_2O)_6$	Mg–O	2.02 (× 2), 2.09 (× 2), 2.11 (× 2)	2.112[a]
	S–O	1.49 (× 4)	1.520[a]
	H–O	0.98–1.00	–
T-$NiSO_4$:$(H_2O)_6$	Ni–O	2.02 (× 2), 2.08 (× 2), 2.09 (× 2)	2.083[a]
	S–O	1.49 (× 4)	1.520[a]
	H–O	0.99–1.00	–
$MgSO_4$:$(H_2O)_7$	Mg–O	2.05 (× 2), 2.06, 2.07, 2.11, 2.14	2.110[a]
	S–O	1.47, 1.48, 1.49, 1.51	1.520[a]
	H–O	0.98–1.00	–
$NiSO_4$:$(H_2O)_7$	Ni–O	2.04, 2.05 (× 3), 2.08, 2.12	2.078[a]
	S–O	1.47, 1.48, 1.49, 1.51	1.520[a]
	H–O	0.99–1.01	–

[a] Average value for all chemical bonds.

possible. Cluster calculations still can answer the question whether the solid phases can be mixed or form a continuous solid solution by comparing the ΔE with kT (kT=25.8 meV, T=300 K). The result from cluster calculations in Fig. 3 (blue crosses) provides an unambiguously answer to the question. Indeed, $\Delta E < kT$ for all cases studied. Therefore, the cluster DFT calculations are in full agreement with the periodic DFT calculations in that both $Ni_xMg_{1-x}SO_4(H_2O)_6$ and $Ni_xMg_{1-x}SO_4(H_2O)_7$ should form a continuous solid solution.

3.3. Charges and charge transfer

To better understand the chemistry of compounds, we calculated the charge of the ions/atoms and the charge transfer between them. In 1971, Bader and Beddal proposed an unambiguous definition of an atom/ion in a molecule/solid by dividing the molecule/solid into spatial regions defining the atoms. The charge on an atom is determined by the number of electrons in its region (Bader and Beddall, 1971; Bader et al., 1981). The boundary of an atom is defined by the zero-flux surfaces between that atom and its neighboring atoms. The Bader charges at the atomic/ionic sites in the related compounds from the periodic DFT calculations are listed in Table 4.

The Bader charges of each element are almost the same for the sulfates, sulfate hydrates, or monoxide. All Mg ions/atoms are more charged compared to the Ni atoms/ions in the same structures, which corresponds to the significantly larger electronegativity of Ni (1.91) than that of Mg (1.31) in the Pauling scale. All the S atoms/ions in the sulfates and their hydrates have almost the same Bader charges (+3.80 to 3.90 e) in spite of the differences between Ni and Mg compounds, which are in agreement with the different electronegativity of 2.58 for S and 3.44 for O. According to the Bader charge analysis, the electronegativity of the $(SO_4)^{2-}$ cluster is significantly higher than that of O from the comparison between MO and $M(SO_4)$ (0.96 vs 1.27 for M=Ni and 1.6 vs 1.7 for M=Mg).

3.4. Electronic properties

Considering the significant structural differences (Fig. 1), it is also interesting to investigate the electronic properties of the Mg and Ni oxides, sulfates, hexa-, and hepta-hydrates. The calculated total density of states (tDOS) for the studied compounds are shown in Fig. 4. Fig. 5 shows the partial density of states (pDOS) of different atoms in selected phases. In Table 5, the electronic energy gaps of the compounds are summarized and compared with the available experimental data.

First we discuss the electronic structure of MgO (Fig. 4a). The ionic nature of this oxide indicates a simple electronic picture with three separate parts: (1) the O 2s states at about 15 eV below the Fermi level which is set as the top of the valence band; (2) the O 2p states dominating the valence band starting from about 5 eV up to the Fermi level; (3) the energy gap between the top of the valence band and the bottom of the conduction band. In this work, the calculated energy band gap of MgO is about 5.25 eV using the optB86-vdW density functional, which is smaller than the experimental value of 7.8 eV (Roessler and Walker, 1967). The eigen-character of the states at the bottom of conduction band for ionic compounds such as MgO was dominated by O 3s states, rather than empty Mg 3s/sp states (de Boer and de Groot, 1998a,b).

The crystal structure of NiO is similar to that of MgO. The only difference is that Ni (electronic configuration of $3d^8$ $4s^2$ in the outer shell) is a 3d transition metal. NiO ($3d^8$) is the prototype of a strongly correlated electron system (Hubbard, 1963; Sawatzky and Allen, 1984; Madsen and Novak, 2005; Larsson, 2006). The van der Waals density functional–GGA calculations shows a metallic behavior even for the antiferromagnetic ordering (Figs. 4b and 5a). Furthermore, in contrast to the experimental observation (Sawatzky and Allen, 1984; Madsen and Novak, 2005; Larsson, 2006), the present calculation shows a low-spin solution with local moment of about 0.45 μ_B/Ni. When we employed the Hubbard U approach with U=5.96 eV and J=0.0 (Hubbard, 1963; Madsen and Novak, 2005), an energy gap of about 2.3 eV was obtained for the anti-ferromagnetic ordering. The Ni ions have

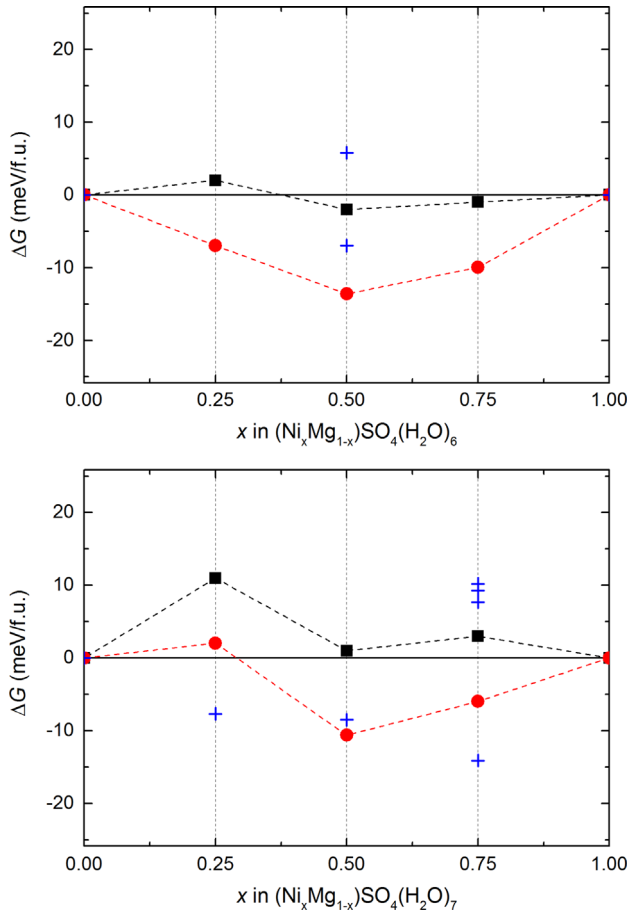

Fig. 3. Relative stability of (a) $(Ni_xMg_{1-x})SO_4(H_2O)_6$ and (b) $(Ni_xMg_{1-x})SO_4(H_2O)_7$ calculated by periodic and cluster DFT calculations. The black squares are the relative formation energy difference ΔE from periodic DFT calculations at 0 K ($\Delta G = \Delta E$, the zero-point vibration energy is ignored); The red circles are those at 300 K with consideration of configuration entropy correction; The blue crosses are the relative total energy difference ΔE from cluster DFT calculations at 0 K ($\Delta G = \Delta E$, the zero-point vibration energy is considered). The scale of the y axes is from 25.85 to −25.85 meV/f.u., corresponding to the value of kT at 300 K. (For interpretation of the references to color in this figure legend, the reader is referred to the web version of this article.)

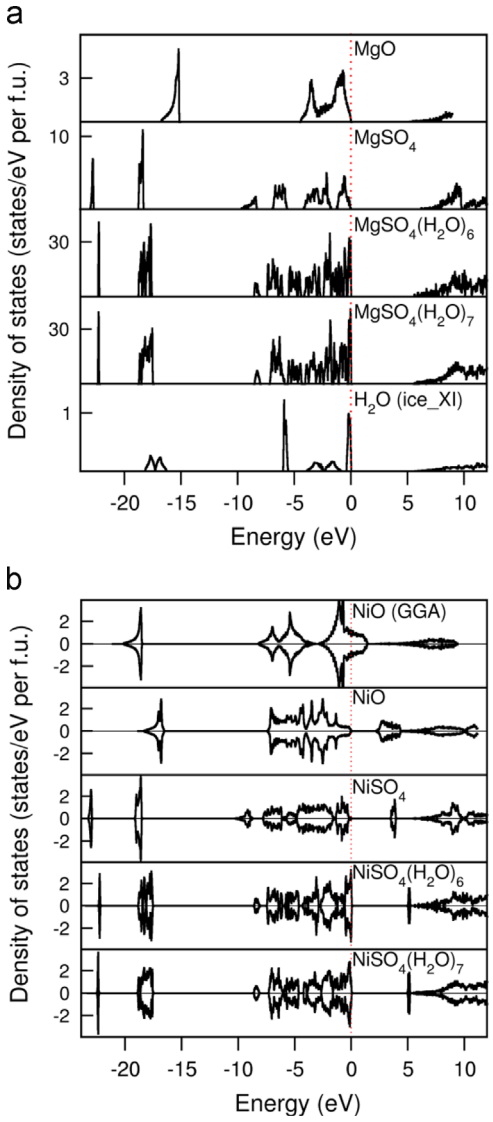

Fig. 4. Total density of states (tDOS) from the periodic DFT calculations for (a) Mg-containing compounds and (b) Ni-containing compounds (AFM ordering) with Hubbard corrections for Ni 3d states.

Table 4
Calculated Bader charges in hydrate metal sulfates and related compounds from the periodic DFT calculations. All charges are in *e*.

Phase	Mg	Ni	S	O	H
Ice_XI	—	—	—	−1.30 to −1.31	~0.65
MgO	1.64	—	—	−1.64	—
NiO	—	0.96	—	−0.96	—
α-$MgSO_4$	1.71	—	3.90	−1.36 to −1.45	—
α-$NiSO_4$	—	1.29	3.87	−1.26 to −1.32	—
β-$MgSO_4$	1.71	—	3.91	−1.38 to −1.41	—
β-$NiSO_4$	—	1.29	3.88	−1.26 to −1.31	—
m-$MgSO_4$:$(H_2O)_6$	1.63	—	3.47	−1.16 to −1.29	0.58–0.65
m-$NiSO_4$:$(H_2O)_6$	—	1.32	3.79	−1.19 to −1.38	0.54–0.69
T-$MgSO_4$:$(H_2O)_6$	1.70	—	3.83	1.31 to −1.38	0.64–0.69
T-$NiSO_4$:$(H_2O)_6$	—	1.26	3.87	−1.24 to −1.30	0.64–0.66
$MgSO_4$:$(H_2O)_7$	1.70	—	3.81	−1.29 to −1.37	0.65–0.68
$NiSO_4$:$(H_2O)_7$	—	1.25	3.80	−1.24 to −1.36	0.64–0.68

high-spin state (2 μ_B/Ni). Although the calculated energy gap is still smaller than the experimental values (about 3.5–4.3 eV) (Sawatzky and Allen, 1984; Madsen and Novak, 2005; Larsson, 2006), the results are greatly improved by the Hubbard U approach (Table 5). For all the Ni-containing phases, our calculations also show that the anti-ferromagnetic solution is more stable. Therefore, all electronic calculations are based on the anti-ferromagnetic ordering for the Ni-containing phases (if possible) in the remainder of the paper.

As shown in Figs. 4 and 5b, the electronic structures of the sulfates are more complex than the oxides. For Mg sulfate, there are six independent bands below the Fermi level. For Ni sulfate, the lowest narrow band at about −23 eV is dominated by S 3s states with some O sp character as well (Fig. 4a). The second lowest band at about −18 eV is composed of O 2s states hybridizing with S 3sp states, which corresponds to the sp3 bonding in the tetragonal coordination in the $(SO_4)^{2-}$ cluster. Such sp3 bonding can also be seen for the third and fourth bands consisting of S 3s and O 2p states (Fig. 4). The top two band for magnesium sulfate (Fig. 4a) are non-bonding O 2p states, while the bands in the same region for the $NiSO_4$ originate from Ni 3d/O 2p mixing with the Ni 3d states dominating the upper part. The calculations give energy gaps for both $MgSO_4$ and $NiSO_4$. However, the nature of the bands are different: for $MgSO_4$, the top of valence band is dominated by (nonbonding) O 2p states and the bottom of the conduction band by O 3s, while for $NiSO_4$, both the top of the valence band and the bottom of the conduction band are dominated by Ni 3d states.

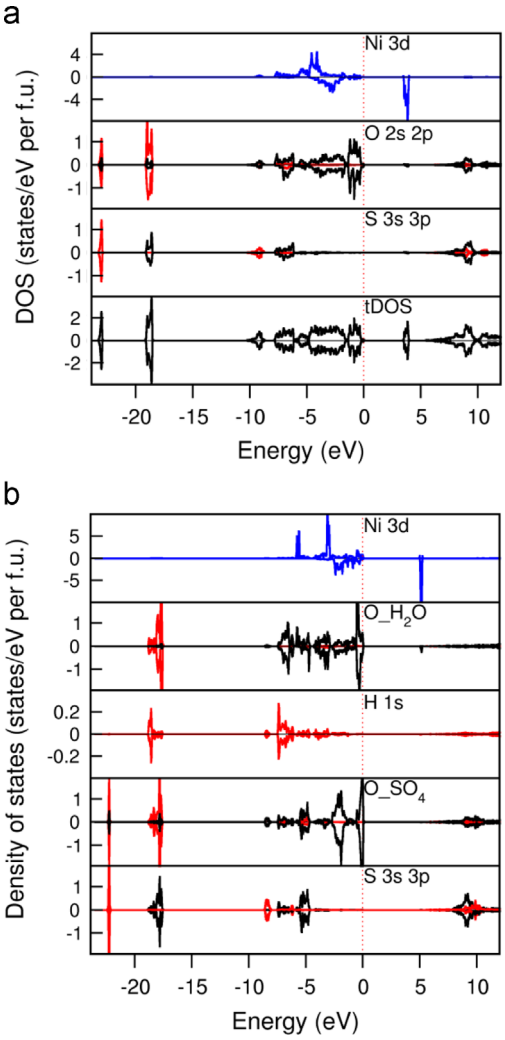

Fig. 5. The partial density of states (pDOS) and total density of states (tDOS) from the periodic DFT calculations for (a) α-$NiSO_4$ and for (b) $NiSO_4(H_2O)_6$ computed using the optB86-vdW+U method. The red, black, and blue lines represent O 2s, O 2p and Ni 3d states, respectively. (For interpretation of the references to color in this figure legend, the reader is referred to the web version of this article.)

Table 5
Calculated energy gaps for MO, MSO_4 (M=Mg or Ni) and the hydrates from the periodic DFT calculations with comparison with available experimental data. The energy gaps are in eV.

Phase	optB86-vdW	+U	Exp.
Ice_XI	5.55	–	8.75[a]
MgO	5.25	–	7.8[b]
NiO	0	2.25	4.3[c]
α-$MgSO_4$	6.02	–	–
α-$NiSO_4$	1.02	3.56	–
β-$MgSO_4$	–	–	–
m-$MgSO_4$:$(H_2O)_6$	5.56	–	–
m-$NiSO_4$:$(H_2O)_6$	1.75	5.14	–
T-$NiSO_4$:$(H_2O)_6$	1.86	5.05	–
$MgSO_4$:$(H_2O)_7$	5.68	–	–
$NiSO_4$:$(H_2O)_7$	1.78	5.24	–

[a] Experimental report in Coe (2001).
[b] Experimental report in Roessler and Walker (1967).
[c] Experimental report in Sawatzky and Allen (1984).

For the hydrated sulfates, the electronic structure is similar to that of anhydrous sulfates as shown in Fig. 4. However, there are some notable differences: (1) the semicore S 3 bands and the Ni 3d bands of the hydrated phases become narrower than those of the corresponding anhydrous phases; (2) The calculated energy gaps of the hydrated Mg sulfates are smaller than that of the anhydrous phase, while for Ni sulfates, the opposite is true due to the longer Ni–Ni distances in the hydrated phases in comparison to the corresponding anhydrous phases.

As is shown in Table 5, the calculated band gaps for all $MSO_4(H_2O)_n$ are relatively large (~5 eV), indicating all these hydrated Mg and Ni sulfates are intrinsically colorless. However, without available experimental data for comparison, the accuracy of the DFT-predicted energy gaps are unclear. DFT functionals in general underestimate the energy gaps of an insulator/semiconductors (Perdew et al., 1996; Madsen and Novak, 2005). The energy gaps calculated with optB86-vdW functionals (standard GGA) for the ice phase and the Mg-compounds are smaller than the experimental values, but in an acceptable range (Table 5). The calculated energy gaps for the Ni-compounds are too small, even for the metallic NiO phase (Table 5). Compared to the standard DFT–GGA method, the optB86-vdW-GGA+U approach significantly improves the calculated energy gaps for the Ni-compounds. However, the differences between DFT calculations and experimental data are significant. For example, the calculated band gap for NiO with Hubbard U approach is smaller than the experimental measurements. Besides the urgent needs of the improved new computational techniques, systematic experimental measurements about the electronic structures of these hydrated transition metal sulfates are worth future investigations.

4. Conclusions

In summary, we presented a comparative first-principles study for a series of Mg and Ni oxides, sulfates and hydrated sulfates, using both periodic and cluster DFT calculations. In the periodic DFT calculations, the van der Waals density functional (optB86-vdW) with Hubbard U for Ni 3d states was used. The calculated lattice parameters of all compounds agree well with the available experimental data. The total energy calculations showed a relatively small energy difference of the Mg substituted configuration of $NiSO_4(H_2O)_n$ (n=6, 7) for all concentrations. The energy differences are typically a few meV/f.u., which are smaller than kT (25.85 meV, T=300 K) indicating the formation of continuous solid solutions at ambient conditions. Considering the cumbersome computing in the periodic DFT calculation, we also investigated the metal sulfates with the computationally less demanding cluster DFT calculations. Though a dimeric or tetrameric cluster contains only a few tens to a few hundred atoms, surprisingly good agreement was found in the calculated results of crystal structures and phase stabilities. This shows that large complex systems such as the hydrated metal sulfates can be efficiently investigated first principles methods. As there is a lack of systematic study of the electronic properties of the Hydrated metal (II) sulfates, we further extended our work to study the electronic structures of these compounds using the periodic DFT calculations. Our electronic structure calculations predict an insulating nature of the compounds. The itinerant nature of the localized Ni 3d states determines largely the electronic properties, in particular the energy gaps of the related phases.

Acknowledgment

This work was sponsored by the Stichting Nationale Computerfaciliteiten (National Computing Facilities Foundation, NCF (MP-213-13)) for the use of supercomputing facilities, with financial support from The Netherlands Organization for Scientific Research (NWO). MAvH acknowledges NWO for a VIDI grant (723.012.006).

References

Abbas, A., Nobbs, D., Romagnoli, J.A., 2002. Investigation of on-line optical particle characterization in reaction and cooling crystallization systems. current state of the art. Meas. Sci. Technol. 13 (3), 349.

Amador, C., Lambrecht, W.R.L., Segall, B., 1992. Application of generalized gradient-corrected density functionals to iron. Phys. Rev. B 46 (3), 1870–1873.

Bader, R.F.W., Beddall, P.M., 1971. Spatial partitioning and transferability of molecular energies. Chem. Phys. Lett. 8 (1), 29–36.

Bader, R.F.W., Nguyendang, T.T., Tal, Y., 1981. A topological theory of molecular-structure. Rep. Prog. Phys. 44 (8), 893–948.

Bartel, L.C., Morosin, B., 1971. Exchange striction in NiO. Phys. Rev. B 3 (3), 1039–1043.

Baur, W.H., 1964. On crystal chemistry of salt hydrates 4. Refinement of crystal structure of $MgSO_4{\cdot}7H_2O$ (Epsomite). Acta Crystallogr. 17 (11), 1361–1369.

Benrath, A., Neumann, E., 1939. Über mischkristalle in der vitriolreihe. V. Ze. Anorg. Allg. Chem. 242 (1), 70–78.

Blochl, P.E., 1994. Projector augmented-wave method. Phys. Rev. B 50 (24), 17953–17979.

Carja, G., Husanu, E., Gherasim, C., Iovu, H., 2011. Layered double hydroxides reconstructed in $NiSO_4$ aqueous solution as highly efficient photocatalysts for degrading two industrial dyes. Appl. Catal. B—Environ. 107 (3–4), 253–259.

Coe, J.V., 2001. Fundamental properties of bulk water from cluster ion data. Int. Rev. Phys. Chem. 20 (1), 33–58.

Cox, W.P., Hornung, E.W., Giauque, W.F., 1955. The spontaneous transformation from macrocrystalline to microcrystalline phases at low temperatures – the heat capacity of $MgSO_4{\cdot}6H_2O$. J. Am. Chem. Soc. 77 (15), 3935–3938.

Dar, F.I., Moonooswamy, K.R., Es-Souni, M., 2013. Morphology and property control of NiO nanostructures for supercapacitor applications. Nanoscale Res. Lett. 8, 363.

de Boer, P.K., de Groot, R.A., 1998a. Conduction bands and invariant energy gaps in alkali bromides. Eur. Phys. J. B 4 (1), 25–28.

de Boer, P.K., de Groot, R.A., 1998b. The conduction bands of MgO, MgS and HfO_2. J. Phys.: Condens. Matter 10 (45), 10241–10248.

Delorme, F., Seron, A., Licheron, M., Veron, E., Giovannelli, F., Beny, C., Jean-Prost, V., Martineau, D., 2009. Synthesis and anion exchange properties of a Zn/Ni double hydroxide salt with a guarinoite structure. J. Solid State Chem. 182 (9), 2350–2356.

Dion, M., Rydberg, H., Schroder, E., Langreth, D.C., Lundqvist, B.I., 2004. Van der Waals density functional for general geometries. Phys. Rev. Lett. 92 (24), 246401.

Fang, C.M., van Huis, M.A., Sluiter, M.H.F., Zandbergen, H.W., 2010. Stability, structure and electronic properties of γ-$Fe_{23}C_6$ from first-principles theory. Acta Mater. 58 (8), 2968–2977.

Fisher, R.A., Hornung, E.W., Brodale, G.E., Giauque, W.F., 1967. Magnetothermodynamics of α-$NiSO_4{\cdot}6H_2O$ I. Heat capacity entropy magnetic moment and internal energy from 0.4° to 4.2° K with fields 0–90 kg along C axis. J. Chem. Phys. 46 (12), 4945–4958.

Fortes, A.D., Wood, I.G., Alfredsson, M., Vocadlo, L., Knight, K.S., 2006. The thermoelastic properties of $MgSO_4{\cdot}7D_2O$ (Epsomite) from powder neutron diffraction and ab initio calculation. Eur. J. Mineral. 18 (4), 449–462.

Fortes, A.D., Wood, I.G., Vocadlo, L., Brand, H.E.A., Knight, K.S., 2007. Crystal structures and thermal expansion of α-$MgSO_4$ and β-$MgSO_4$ from 4.2 to 300 K by neutron powder diffraction. J. Appl. Crystallogr. 40, 761–770.

Frazer, B.C., Brown, P.J., 1962. Antiferromagnetic Structure of Crvo4 and anhydrous sulfates of divalent Fe, Ni, and Co. Phys. Rev. 125 (4), 1283–1291.

Frondel, C., Palache, C., 1949. Retgersite, $NiSO_4{\cdot}6H_2O$ a new mineral. Am. Mineral. 34 (3–4), 188–194.

Grevel, K.D., Majzlan, J., 2009. Internally consistent thermodynamic data for magnesium sulfate hydrates. Geochim. Cosmochim. Acta 73 (22), 6805–6815.

Hawthorne, F., 2012. A bond-topological approach to theoretical mineralogy: crystal structure, chemical composition and chemical reactions. Phys. Chem. Miner. 39 (10), 841–874.

Hehre, W.J, 2003. A Gudie to Molecular Mechanics and Quantum Chemical Calculations. Wavefunction Inc.

Hubbard, J., 1963. Electron correlations in narrow energy bands. Proc. R. Soc. Lond. Ser. A—Math. Phys. Sci. 276 (1364), 238–257.

Iype, E., Nedea, S.V., Rindt, C.C.M., van Steenhoven, A.A., Zondag, H.A., Jansen, A.P.J., 2012. DFT study on characterization of hydrogen bonds in the hydrates of $MgSO_4$. J. Phys. Chem. C 116 (35), 18584–18590.

Kavitha, J.M., Mahadevan, C.K., 2013. Growth and characterization of pure glycine added morenosite single crystals. Int. J. Eng. Res. Appl. 3 (5), 1931–1940.

Klimes, J., Bowler, D.R., Michaelides, A., 2010. Chemical accuracy for the van der Waals density functional. J. Phys.-Condens. Matter 22 (2), 022201.

Klimes, J., Bowler, D.R., Michaelides, A., 2011. Van der Waals density functionals applied to solids. Phys. Rev. B 83 (19), 195131.

Koga, N., Tanaka, H., 1994. Kinetic and morphological-studies of the thermal dehydration of α-nickel (ii) sulfate hexahydrate. J. Phys. Chem. 98 (41), 10521–10528.

Kresse, G., Hafner, J., 1993. Abinitio molecular-dynamics for liquid-metals. Phys. Rev. B 47 (1), 558–561.

Kresse, G., Hafner, J., 1994. Ab-initio molecular-dynamics simulation of the liquid-metal amorphous-semiconductor transition in germanium. Phys. Rev. B 49 (20), 14251–14269.

Kresse, G., Joubert, D., 1999. From ultrasoft pseudopotentials to the projector augmented-wave method. Phys. Rev. B 59 (3), 1758–1775.

Larsson, S., 2006. Localization of electrons and excitations. Chem. Phys. 326 (1), 115–122.

Lascelles, K., Morgan, L.G., Nicholls, D., Beyersmann, D., 2005. Nickel compounds, Ullmann's Encyclopedia of Industrial Chemistry. Wiley-VCH Verlag GmbH & Co. KGaA.

Leadbetter, A.J., Ward, R.C., Clark, J.W., Tucker, P.A., Matsuo, T., Suga, H., 1985. The equilibrium low-temperature structure of ice. J. Chem. Phys. 82 (1), 424–428.

Lu, X., Genceli-Güner, F.E., van Spronsen, J., Oosterhof, H., Witkamp, G.J., 2014a. Eutectic freeze crystallization of nickel sulfate from an industrial stream: a comparison with evaporative crystallization. Hydrometallurgy (in preparation).

Lu, X., van Spronsen, J., Genceli-Güner, F.E., Witkamp, G.J., 2014b. Recrystallization of nickel sulfate products from industrial solution. Hydrometallurgy (in preparation).

Luo, J.H., Zhang, Y.H., Li, Z.S., 2013. Adsorption of water on an $MgSO_4$ (100) surface: a first-principles investigation. ChemPhysChem 14 (9), 1969–1976.

Madsen, G.K.H., Novak, P., 2005. Charge order in magnetite. An LDA+U study. Europhys. Lett. 69 (5), 777–783.

Maneva, M., Rizova, D., Genov, L., Liptay, G., 1990. On the thermal-decomposition of $NiSO_4{\cdot}7H_2O$, $NiSO_4{\cdot}6H_2O$, $NiSO_4{\cdot}4H_2O$, $NiSO_4{\cdot}1H_2O$ and of their deuterated analogs. J. Therm. Anal. 36 (3), 915–922.

Maslyuk, V.V., Tegenkamp, C., Pfnur, H., Bredow, T., 2005. Properties of ternary insulating systems: the electronic structure of $MgSO_4{\cdot}H_2O$. J. Phys. Chem. A 109 (18), 4118–4124.

Moldoveanu, G., Demopoulos, G., 2002. Producing high-grade nickel sulfate with solvent displacement crystallization. JOM 54 (1), 49–53.

Monkhorst, H.J., Pack, J.D., 1976. Special points for brillouin-zone integrations. Phys. Rev. B 13 (12), 5188–5192.

Nesbitt, H.W., Legrand, D., Bancroft, G.M., 2000. Interpretation of Ni 2p XPS spectra of Ni conductors and Ni insulators. Phys. Chem. Miner. 27 (5), 357–366.

Nordstrom, D.K., 2009. Acid rock drainage and climate change. J. Geochem. Explor. 100 (2-3), 97–104.

O'Connor, J.J., Beck, C., Underwood, N., 1941. Magnetic rotatory power of crystalline nickel sulfate in the ultraviolet region. Phys. Rev. 60 (6), 443–447.

Osborne, H.C., 1947. Nickelian epsomite from North Auckland, New Zealand. Am. Mineral. 32 (9-10), 553–560.

Paterson, H.B.W., 1994. Hydrogenation of Fats and Oils: Theory and Practice. American Oil Chemists Society.

Perdew, J.P., Burke, K., Ernzerhof, M., 1996. Generalized gradient approximation made simple. Phys. Rev. Lett. 77 (18), 3865–3868.

Pontusch, W.M., Piccini, A., Quadros, C.J.A., Isotani, S., 1973. EPR measurements on single-crystals of α-$NiSO_4{\cdot}6H_2O$. Phys. Lett. A 44 (1), 57–58.

Ptasiewicz-Bak, H., Olovsson, I., McIntyre, G.J., 1993. Bonding deformation and superposition in the electron density of tetragonal $NiSO_4{\cdot}6H_2O$ at 25 K. Acta Crystallogr. Sect. B 49 (2), 192–201.

Ramachandran, P., Venkateswaran, K.V., Visvanathan, S., 1991. The electrochemical recovery of nickel from plating residues. JOM 43 (6), 34–36.

Roessler, D.M., Walker, W.C., 1967. Electronic spectrum and ultraviolet optical properties of crystalline MgO. Phys. Rev. 159 (3), 733–738.

Spartan 14.Wavefunction Inc., Von Karman Avenue, Suite 370, Irvine CA 92612 www.wavefun.com.

Sawatzky, G.A., Allen, J.W., 1984. Magnitude and origin of the band-gap in NiO. Phys. Rev. Lett. 53 (24), 2339–2342.

Schlapp, R., Penney, W.G., 1932. Influence of crystalline fields on the susceptibilities of salts of paramagnetic ions. II. The Iron group, especially Ni, Cr and Co. Phys. Rev. 42 (5), 0666–0686.

Schröder, D., Ducháčková, L., Tarábek, J., Karwowska, M., Fijalkowski, K.J., Ončák, M., Slavíček, P., 2011. Direct observation of triple ions in aqueous solutions of nickel (II) sulfate: a molecular link between the gas phase and bulk behavior. J. Am. Chem. Soc. 133 (8), 2444–2451.

Smolik, M., 2000. Distribution of trace amounts of M^{2+} ions during crystallization of $NiSO_4 \cdot 7H_2O$. Pol. J. Chem. 74 (10), 1447–1461.

Squyres, S.W., Grotzinger, J.P., Arvidson, R.E., Bell, J.F., Calvin, W., Christensen, P.R., Clark, B.C., Crisp, J.A., Farrand, W.H., Herkenhoff, K.E., Johnson, J.R., Klingelhofer, G., Knoll, A.H., McLennan, S.M., McSween, H.Y., Morris, R.V., Rice, J.W., Rieder, R., Soderblom, L.A., 2004. In situ evidence for an ancient aqueous environment at Meridiani Planum, Mars. Science 306 (5702), 1709–1714.

Stout, J.W., Hadley, W.B., 1964. Heat capacity of α-$NiSO_46H_2O$ between 1 and 20 K: electronic energy levels of Ni^{++} ion. J. Chem. Phys. 40 (1), 55.

Swift, T.J., Connick, R.E., 1962. NMR-relaxation mechanisms of O_{17} in aqueous solutions of paramagnetic cations and the lifetime of water molecules in the first coordination sphere. J. Chem. Phys. 37 (2), 307–320.

Watanabe, T., 1962. Magnetic properties of $NiSO_4{\cdot}7H_2O$ and alpha-$NiSO_4{\cdot}6H_2O$ at low temperatures. J. Phys. Soc. Jpn. 17 (12), 1856–1864.

Wells, A.F., 1984. Structural Inorganic Chemistry. Clarendon Press, Oxford.

Wildner, M., 1990. Crystal structure refinements of $CoSO_4$ and $NiSO_4$: very short interpolyhedral O–O contacts. Ze. Kristallogr. 191, 223–229.

Wyckoff, R.W.G., 1921. The crystal structure of magnesium oxide. Am. J. Sci. 1 (2), 138–152.

Zalkin, A., Templeton, D.H., Ruben, H., 1964. Crystal structure+hydrogen bonding of magnesium sulfate hexahydrate. Acta Crystallogr. 17 (3), 235–240.